Mathematical modeling

Математическое моделирование

UDC 51-74:621.791.92
https://doi.org/10.32362/2500-316X-2025-13-6-127-138
EDN ORZKBC

RESEARCH ARTICLE

Unsteady heat transfer problem during single-pass spraying on a half-space

Mikhail E. Soloviev [1, @], Sergey S. Kokarev [2], Sergey L. Baldaev [3], Lev Kh. Baldaev [3], Denis V. Malyshev [1]

[1] *Yaroslavl State Technical University, Yaroslavl, 150023 Russia*
[2] *Regional Scientific and Educational Center "Logos," Yaroslavl, 150000 Russia*
[3] *Technological Systems for Protective Coatings, Moscow, Shcherbinka, 108851 Russia*
[@] *Corresponding author, e-mail: me_s@mail.ru*

• **Submitted:** 26.03.2025 • **Revised:** 18.05.2025 • **Accepted:** 06.10.2025

Abstract

Objectives. Thermal spraying and powder laser cladding are promising technologies widely used in various industries, including aerospace, energy, and mechanical engineering. The efficiency of these technologies depends on the management of thermal processes occurring during coating application, which directly affect the quality and durability of the resulting materials and products. This article considers a nonstationary problem of heat transfer during single-pass spraying on a half-space. The research aim was to simulate the temperature distribution in a material half-space upon the action of a moving heat source on its boundary.

Methods. A theoretical study of the temperature distribution on the surface and in the bulk of the processed material during movement of the spray head was carried out by solving the equation of nonstationary thermal conductivity in Cartesian coordinates. This equation employs a special type of the heat source power density function in the form of a thermal strip, simulating the process of heat transfer from the spray path to the material half-space of the part base.

Results. The obtained solution representing the evolution of temperature in time at different points of the medium shows that at a certain point of time after the passage of the heating pulse, the temperature inside the medium reaches its maximum value rapidly followed by its relatively slow relaxation to the equilibrium temperature of the environment. Penetrating deeper into the bulk of the medium, the thermal pulse is spreading out while decreasing its amplitude and increasing its width, accompanied by a monotonic increase in the time to reach the maximum. The transverse temperature distribution has the form of symmetrical peaks, less pronounced in depth.

Conclusions. The obtained solution can be used when describing the general temperature field at some distance from the spray head area, where specific heating details are lacking. In particular, the work shows that significant temperature gradients arise in the vicinity of the primary spray area, which will cause noticeable nonstationary temperature stresses.

Keywords: gas-thermal spraying, powder laser cladding, nonstationary heat conduction equation, temperature field, temperature wave, Newton–Richmann boundary conditions, Green's function for the heat equation

For citation: Soloviev M.E., Kokarev S.S., Baldaev S.L., Baldaev L.Kh., Malyshev D.V. Unsteady heat transfer problem during single-pass spraying on a half-space. *Russian Technological Journal.* 2025;13(6):127–138. https://doi.org/10.32362/2500-316X-2025-13-6-127-138, https://www.elibrary.ru/ORZKBC

Financial disclosure: The authors have no financial or proprietary interest in any material or method mentioned.

The authors declare no conflicts of interest.

НАУЧНАЯ СТАТЬЯ

Нестационарная задача теплопроводности в технологии газотермического напыления защитных покрытий

М.Е. Соловьев [1, @], С.С. Кокарев [2], С.Л. Балдаев [3], Л.Х. Балдаев [3], Д.В. Малышев [1]

[1] *Ярославский государственный технический университет, Ярославль, 150023 Россия*
[2] *Региональный научно-образовательный центр «Логос», Ярославль, 150000 Россия*
[3] *ООО «Технологические системы защитных покрытий», Москва, Щербинка, 108851 Россия*
[@] *Автор для переписки, e-mail: me_s@mail.ru*

• **Поступила:** 26.03.2025 • **Доработана:** 18.05.2025 • **Принята к опубликованию:** 06.10.2025

Резюме

Цели. Газотермическое напыление и порошковая лазерная наплавка – перспективные технологии, широко применяемые в различных отраслях промышленности, включая аэрокосмическую, энергетическую и машиностроительную отрасли. Одним из ключевых аспектов данных технологий является управление тепловыми процессами, возникающими при нанесении покрытий, т.к. они напрямую влияют на качество и долговечность получаемых материалов и изделий. В данной статье рассматривается нестационарная задача теплопереноса при однопроходном напылении на полупространство. Целью работы является моделирование распределения температуры в материальном полупространстве, на границе которого действует движущийся источник тепла.

Методы. Теоретическое исследование распределения температуры на поверхности и в толще обрабатываемого материала в процессе движения головки распылителя осуществлялось путем решения уравнения нестационарной теплопроводности в декартовых координатах. Особенностью уравнения является специальный вид функции плотности мощности источника тепла в виде тепловой полосы, моделирующей процесс теплопередачи от дорожки напыления в материальное полупространство основы детали.

Результаты. В результате исследования полученного решения, представляющего эволюцию во времени температуры в различных точках среды, установлено, что через некоторое время после прохождения импульса нагревания температура внутри среды довольно быстро достигает максимального значения, а затем она относительно медленно релаксирует к равновесной температуре окружающей среды. По мере углубления в толщу среды тепловой импульс расплывается, уменьшается его амплитуда и увеличивается ширина, а время достижения максимума монотонно увеличивается. Поперечное распределение температуры имеет вид симметричных пиков, менее выраженных в глубине.

Выводы. Полученное решение может быть полезным при описании общего температурного поля на некотором удалении от области действия головки распылителя, где конкретные детали нагрева не проявляются. В частности, в работе показано, что в окрестности действия первичной области напыления возникают значительные градиенты температур, которые вызывают заметные нестационарные температурные напряжения.

Ключевые слова: газотермическое напыление, порошковая лазерная наплавка, нестационарное уравнение теплопроводности, температурное поле, температурная волна, граничные условия Ньютона – Рихмана, функция Грина для уравнения теплопроводности

Для цитирования: Соловьев М.Е., Кокарев С.С., Балдаев С.Л., Балдаев Л.Х., Малышев Д.В. Нестационарная задача теплопроводности в технологии газотермического напыления защитных покрытий. *Russian Technological Journal*. 2025;13(6):127–138. https://doi.org/10.32362/2500-316X-2025-13-6-127-138, https://www.elibrary.ru/ORZKBC

Прозрачность финансовой деятельности: Авторы не имеют финансовой заинтересованности в представленных материалах или методах.

Авторы заявляют об отсутствии конфликта интересов.

INTRODUCTION

In modern mechanical engineering, powder coating technologies using gas-thermal spraying [1, 2] and laser cladding [3, 4] are widely used. These methods enable not only the effective restoration of worn parts surfaces, but also the creation of specialized coatings with a unique set of characteristics, including increased heat, wear, and chemical resistance [5, 6]. Laser cladding has also become a fundamental technology in the field of additive manufacturing of metal products, where parts are produced by applying powder material layer by layer [7, 8].

These technologies involve heating powdered materials to temperatures exceeding their melting point, followed by application to the surface of the part using a high-speed gas flow. A distinctive feature of laser cladding is the use of an infrared laser as a source of particle heating. The laser beam is focused on the surface of the part or in its close proximity, which provides for a more accurate control of the temperature of the deposited material and precise positioning of the deposition path. In the case of conventional gas-thermal spraying, the material is heated directly in the spray head. The basic technological operation of these processes is a single pass of the plasma torch along the surface being treated, resulting in the appearance of a single thin molten track on this surface at a speed equal to that of the plasma torch. In this work, we focus on this basic operation due to its determining effect on the quality of the coating.

Optimization of the technologies under consideration with the purpose of enhancing the quality of the coatings and products obtained requires elucidation of those thermophysical processes that occur when molten material interacts with the surface being treated [9–11]. In particular, the temperature distribution across the substrate material during and after the passage of the spray head is of particular interest [12]. The importance of precise heat input control for obtaining the desired coating microstructure was also underscored in [13, 14].

Mathematical modeling methods are widely used to optimize spraying technologies and predict the properties of the coatings being formed [15–17]. Numerical methods, such as the finite element method [13, 18, 19], are used to model the temperature distribution in the spray path. The authors of [20] used the finite volume method to investigate the influence of temperature distribution during laser cladding on the melting process of powdered metal in the cladding path and the influence of the Marangoni effect on the size of the melting zone. This method was also used in [21] for numerical simulation of heat and mass transfer processes in a three-dimensional problem setting when simulating powder laser cladding of stainless steel. It was shown that the temperature distribution in the cladding track is a critical factor determining the shape of its cross-section profile. In addition to the power of the radiation source, the temperature distribution in the deposition track is influenced by the speed of the deposition head relative to the sample surface and the powder flow rate [22, 23].

Along with numerical methods, analytical methods can also be used to describe a moving heat source, predict the cooling rate [13, 24], and estimate the shape of the molten metal pool [25].

When the focus is heat transfer processes during spraying, rather than a detailed distribution of thermal quantities in the track volume and their dynamics over time, simplified models can be applied. In these models, spraying generates a localized source of heat along the plasma jet line of action and localized in time. In further research, such a model can be taken as a zero (main) approximation, and all other details of the process can be taken into account in the form of corrections, in which the parameter of smallness will be the ratio of the track width to the characteristic size of the treated surface.

In this article, we consider the problem of nonstationary temperature distribution in an infinite homogeneous half-space, the boundary of which features a time-growing "heat line." This line is a heat source localized on a geometric ray, the origin of which moves along a flat boundary at a constant speed. In such a formulation, the problem is somewhat non-standard, since its initial conditions are

replaced by an asymptotic condition for the temperature field: as $t \to -\infty$, the temperature field of the half-space tends to a constant value—the ambient temperature.

TASK STATEMENT

Abstracting from the size and shape of the sprayed surface, let us consider this surface as the boundary of an infinite half-space filled with a heat-conducting substance with constant thermal conductivity α and specific volumetric heat capacity c. On this surface, let us consider a continuously growing thermal strip with a velocity $\vec{v}$ consisting of point instantaneous heat sources with a heat energy output $q_0(t)$ as a certain decreasing function of time (Fig. 1).

The axes of the fixed coordinate system are oriented as shown in Fig. 1. In the selected coordinate system, the power density of heat sources of the type under consideration is described by the ratio

$$q(t, x, y, z) = q_0(t, x)\delta(z)\delta(y)\delta(x - vt), \quad (1)$$

wherein δ is the Dirac delta function. The conditional moment $t = 0$ is shown in Fig. 1. The conditional moment $t = 0$ does not correspond to any initial conditions, since the thermal band begins to form at $t \to -\infty$

In the model under consideration, the function $q_0(t, x)$ is defined externally. Thus, it simulates the process of heat transfer from the thermal strip to the material of the half-space and depends on many physical parameters in the spraying process. In this article, we use the simplest model of "stepwise thermal illumination," in which

$$q_0(t, x) = \mathrm{k}(\theta(t - x/v) - \theta(t - x/v - \tau)), \quad (2)$$

wherein k is the constant effective thermal power of illumination; τ is the effective thermal illumination time (the effective values represent a simplified model of heat exchange along a line of heat sources, in which the heat source moves along the line at the speed of light and transfers heat to the material of the half-space with a constant power k during a finite time interval τ at each point along the line of sources); $\theta(x)$ is the standard Heaviside step function.

The heat conduction equation for the problem under consideration will take the form

$$\dot{T} - \alpha\Delta T = \\ = p\delta(y)\delta(z)\delta(x - vt)(\theta(t - x/v) - \theta(t - x/v - \tau)), \quad (3)$$

wherein T is the temperature in the region under consideration, α is the thermal conductivity coefficient, $p = \mathrm{k}/c$, and the range of the variables changing is $(x, y) \in \mathbb{R}^2$, $z \in (-\infty, 0)$, $t \in \mathbb{R}$.

Equation (3) must be supplemented with Newton–Richman boundary conditions, specified at the boundary of the half-space in the form

$$\left.\frac{-\partial T}{\partial z}\right|_{z=0} = \beta\left(T\big|_{z=0} - T_0\right), \quad (4)$$

wherein β is the reduced heat transfer coefficient, equal to the ratio of the heat transfer coefficient at the material-air interface to the thermal conductivity of the material; T_0 is the ambient (air) temperature, which coincides with the temperature in the asymptotic initial condition; the minus sign on the left side corresponds to cooling

$$T\big|_{t\to\infty} = T_0 = \mathrm{const}, \quad (5)$$

playing the role of the initial condition in the formulation of the problem under consideration and necessary for its correct formulation.

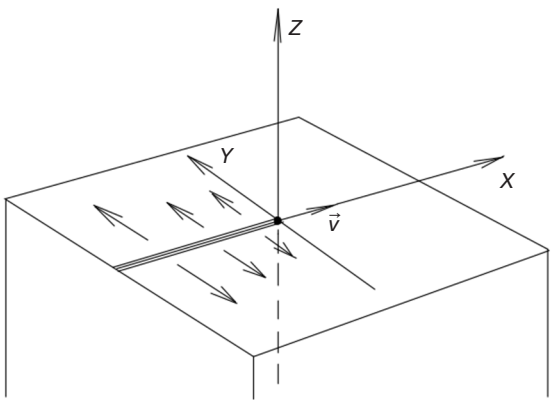

Fig. 1. Thermal strip on the surface of a semi-infinite material half-space

SOLUTION OF A NON-HOMOGENEOUS EQUATION

We will seek a particular solution to the inhomogeneous equation (3) using Green's function G for the heat conductivity operator

$$\left(\frac{\partial}{\partial t'} - \alpha\Delta'\right)G(t-t',\vec{r}-\vec{r}') = \delta(t-t')\delta^3(\vec{r}-\vec{r}'), \tag{6}$$

which, with arbitrary precision, is determined by the formula for solving a homogeneous equation

$$G(t-t',\vec{r}-\vec{r}') = \frac{1}{(2\sqrt{\alpha\pi(t-t')})^3}\mathrm{e}^{-|\vec{r}-\vec{r}'|^2/4\alpha(t-t')}\theta(t-t'), \tag{7}$$

wherein $\vec{r}$ corresponds to the current point (x, y, z).

The particular solution $\overline{T}(t,\vec{r})$ of the equation (3) corresponding to (7) takes the form

$$\overline{T}(t,\vec{r}) = \int_{-\infty}^{t} dt' \int_{\mathbb{R}^3} d^3\vec{r}' \frac{1}{\left(2\sqrt{\alpha\pi(t-t')}\right)^3}\mathrm{e}^{-((x-x')^2+(y-y')^2+(z-z')^2)/4\alpha(t-t')} \times \\ \times p\delta(y')\delta(z')\delta(x'-vt')(\theta(t'-x'/v)-\theta(t'-x'/v-\tau)). \tag{8}$$

Integrating over y', z' leads to the following intermediate formula for the particular solution:

$$\overline{T}(t,\vec{r}) = \frac{p}{\left(2\sqrt{\alpha\pi}\right)^{3/2}} \int_{-\infty}^{t} dt' \int_{-\infty}^{+\infty} dx' \frac{\mathrm{e}^{-((x-x')^2+y^2+z^2)/4\alpha(t-t')}}{(t-t')^{3/2}} \times \\ \times \delta(x'-vt')(\theta(t'-x'/v)-\theta(t'-x'/v-\tau)). \tag{9}$$

For correct integration over variables (x, t), we will proceed to lagging and leading combinations of the initial variables:

$$r = x'-vt',\ s = x'+vt' \Leftrightarrow t' = \frac{s-r}{2v},\ x' = \frac{s+r}{2}. \tag{10}$$

The volume element will be replaced according to the rule $dt'dx' = ds\,dr/2v$, the integration region (in coordinates x', t' representing a half-plane $t' \le t$) will become a half-plane $s - r - 2vt \le 0$.

In the new variables, integral (9) will take the form

$$\overline{T}(t,\vec{r}) = \frac{p}{2v\left(2\sqrt{\alpha\pi}\right)^{3/2}} \int_{-\infty}^{+\infty} ds \int_{s-2vt}^{+\infty} dr \frac{\mathrm{e}^{-((x-(s+r)/2)^2+y^2+z^2)/4\alpha(t-(s-r)/2v)}}{(t-(s-r)/2v)^{3/2}} \times \\ \times \delta(r)(\theta(-r/v)-\theta(-r/v-\tau)). \tag{11}$$

Integrating over variable r instead of function δ gives 0 if $s - 2vt > 0$ and 1 if the opposite additional equality holds when substituting $r = 0$ into all occurrences of variable r This situation is universally described by the factor $\theta(2vt - s)$, which ultimately leads to the integral

$$\overline{T}(t,\vec{r}) = \\ = \frac{p}{2v\left(2\sqrt{\alpha\pi}\right)^{3/2}} \int_{-\infty}^{+\infty} ds \frac{\mathrm{e}^{-((x-s/2)^2+y^2+z^2)/4\alpha(t-s/2v)}}{(t-s/2v)^{3/2}}\theta(2vt-s) = \frac{p}{2v\left(2\sqrt{\alpha\pi}\right)^{3/2}} \int_{-\infty}^{2vt} ds \frac{\mathrm{e}^{-((x-s/2)^2+y^2+z^2)/4\alpha(t-s/2v)}}{(t-s/2v)^{3/2}}. \tag{12}$$

Let us introduce a new variable $u = t - s/2v$, for which the integral will take the form

$$\overline{T}(t,\vec{r}) = \frac{p}{\left(2\sqrt{\alpha\pi}\right)^{3/2}} \int_0^{+\infty} du \frac{e^{-((x-v(t-u))^2 + y^2 + z^2)/4\alpha u}}{u^{3/2}}. \quad (13)$$

Integral (13) is calculated in elementary functions, and the final result is as follows:

$$\overline{T}(t,\vec{r}) = \frac{p}{4\alpha\pi} \cdot \frac{e^{-\left(\sqrt{(x-vt)^2 + y^2 + z^2} + x - vt\right)v/2\alpha}}{\sqrt{(x-vt)^2 + y^2 + z^2}}. \quad (14)$$

In fact, solution (14) describes an axially symmetric thermal wave whose center moves at a speed v along the x axis. In the accompanying inertial reference frame $x = vt$ formula (14) takes the form of a cylindrical wave

$$\overline{T}'(t,\vec{r}) = \frac{p}{4\alpha\pi} \cdot \frac{e^{-\rho v/2\alpha}}{\rho}, \quad (15)$$

wherein $\rho = \sqrt{y^2 + z^2}$, with an axis coinciding with the line of heat sources.

When $t \to \pm\infty$ solution (13) tends to zero for various reasons. When $t \to -\infty$, the heat has not yet been released. However, when $t \to +\infty$, the infinite heat released along the entire thermal line has time to relax over an infinite volume, which, as a result, returns to a state of zero temperature. At a typical point at a certain distance ρ from the thermal axis, the evolution of temperature over time is shown in Fig. 2. It has the form of a thermal pulse that increases rapidly immediately after the passage of the thermal pulse activation wave on the thermal line (the moment when the laser beam passes the observation point at coordinate $x = 0$) and relatively slowly (according to the law of inverse proportionality) relaxes to a state of equilibrium with zero temperature. The solution obtained does not have any physical meaning yet relevant to the task at hand: this solution must be supplemented with a general solution of the homogeneous equation, with the help of which the boundary conditions (4) can be implemented (4).

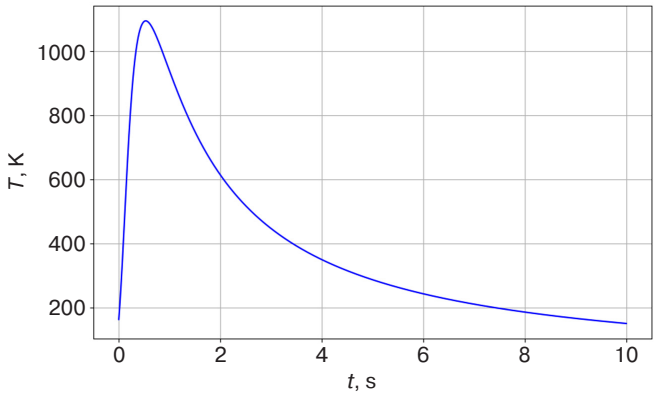

Fig. 2. Dependence $T(t)$ at parameter values: $x = 0$, $y = 1$, $z = 1$ (in mm), $v = 5$ mm/s, $\alpha = 1$ mm^2/s, $p = 1.0 \cdot 10^5$ mm^3·K/s

SOLUTION OF A HOMOGENEOUS EQUATION AND COMPLETE SOLUTION

Due to the linearity of heat conduction equation (3), its general solution can be written as the sum of a particular solution of a non-homogeneous equation and the general solution of a homogeneous equation T_h:

$$T(t,x,y,z) = \overline{T}(t,x,y,z) + T_h(t,x,y,z), \quad (16)$$

wherein $\overline{T}$ is the particular solution (14) already found in the previous section. In this section, we will find a suitable T_h. In essence, it is reduced to implementing the selected boundary condition (4) using T_h. Substituting expression (16) therein, after regrouping the summands, we find

$$\left(\beta T_{\text{h}} + \frac{\partial T_{\text{h}}}{\partial z}\right)\Bigg|_{z=0} = \beta\left(T_0 - \overline{T}\right)\Big|_{z=0}, \tag{17}$$

wherein the right-hand side is the already known function. In addition, it was taken into account that, due to the evenness of $\overline{T}$ by z, the following equality holds: $\left.\frac{\partial T_{\text{h}}}{\partial z}\right|_{z=0} = 0.$

We will seek a common solution T_{h} using the method of separation of variables:

$$T_{\text{h}} = \Theta(t)X(x)Y(y)Z(z). \tag{18}$$

Substituting (18) into equation (3) at $p = 0$ and dividing it by T_{h}, we obtain the heat conduction equation in a separated form:

$$\frac{\Theta'}{\Theta} - \alpha\left(\frac{X''}{X} + \frac{Y''}{Y} + \frac{Z''}{Z}\right) = 0, \tag{19}$$

wherein the stroke denotes differentiation with respect to the argument. The condition for separating variables takes the form of constancy of individual terms in (19); hence, this equation expresses the relationship between the separation constants

$$k_t - \alpha\left(-k_x^2 - k_y^2 + k_z^2\right) = 0, \tag{20}$$

which we will understand as an expression for the wave number k_z:

$$k_z = \pm\sqrt{\frac{k_t}{\alpha} + k_x^2 + k_y^2}. \tag{21}$$

In (20)

$$k_t = \frac{\Theta'}{\Theta},\ \frac{X''}{X} = -k_x^2\ \frac{Y''}{Y} = k_y^2,\ \frac{Z''}{Z} = k_z^2. \tag{22}$$

The general solution T_{h} has the following decomposition (a linear combination of different solutions with constant coefficients):

$$T_{\text{h}} = \sum_{k,\varepsilon} C_{k,\varepsilon} \mathrm{e}^{k_t t + i(k_x x + k_y y) + \varepsilon\sqrt{k_t/\alpha + k_x^2 + k_y^2}\, z}, \tag{23}$$

wherein $k = \{k_t, k_x, k_y\}$, and the parameter $\varepsilon = \pm 1$ distinguishes the roots for k_z в (21).

In order to find the Fourier coefficients $C_{k,\,\varepsilon}$ we substitute expression (23) into boundary condition (17), in which we also transform the right-hand side into a Fourier integral. All Fourier transforms will be greatly simplified when noting that in the right side of (17), the particular solution $\overline{T}$ depends, according to (14), only on the lagging combination $\xi = x - vt$. In order for the same combination to appear in the left side of (17), it is necessary and sufficient to require that $k_t = -ivk_x$. Only in this case will the desired combination $ik_x(x - vt) = ik_\xi\xi$ be formed in the exponent on the left, relative to which the Fourier transform will be calculated. This leads to a correct dependence on the right-hand side. Let us find the Fourier image of the right side of (17). We have a chain of equalities $\left(a + v/2\alpha,\ K = \sqrt{k_y^2 + k_\xi^2}\right)$:

$$\begin{aligned}
&\frac{1}{(2\pi)^2}\int\limits_{\mathbb{R}^2} d\xi\, dy\, \beta\left(T_0 - \frac{p}{4\pi\alpha}\cdot\frac{\mathrm{e}^{-\left(\sqrt{\xi^2+y^2}+\xi\right)v/2\alpha}}{\sqrt{\xi^2+y^2}}\right)\mathrm{e}^{-i\left(k_\xi\xi + k_y y\right)} \overset{\{\xi=\rho\cos\varphi,\ y=\rho\sin\varphi\}}{=} \\
&= \beta T_0\delta(k_\xi)\delta(k_y) - \frac{\beta p}{16\pi^3\alpha}\int\limits_0^{2\pi} d\varphi\int\limits_0^{\infty}\rho d\rho\cdot\frac{\mathrm{e}^{-a(\rho+\rho\cos\varphi)}}{\rho}\mathrm{e}^{-iK\rho\cos(\psi-\varphi)} = \\
&= \beta T_0\delta(k_\xi)\delta(k_y) - \frac{\beta p}{16\pi^3\alpha}\int\limits_0^{2\pi}\frac{d\varphi}{a(1+\cos\varphi) + iK\cos(\psi-\varphi)} \equiv F(k_y, k_\xi).
\end{aligned} \tag{24}$$

The integral in the latter expression is calculated using the analytical continuation of the real formula

$$\int_0^{2\pi} \frac{d\varphi}{a + b\cos\varphi + c\cos\varphi} = \frac{2\pi}{\sqrt{a^2 - b^2 - c^2}} \tag{25}$$

into a complex domain, which, in our case, gives the equality

$$\int_0^{2\pi} \frac{d\varphi}{a(1+\cos\varphi) + iK\cos(\psi - \varphi)} = \frac{2\pi}{\sqrt{K^2 - 2iak_\xi}} \tag{26}$$

with the choice of the root branch that gives $\sqrt{K^2} = k_y$ when $k_\xi = 0$.

Finally, for the Fourier image of the right side (17), we obtain:

$$F(k_y, k_\xi) = \beta T_0 \delta(k_\xi)\delta(k_y) - \frac{\beta p}{8\pi^2\alpha\sqrt{K^2 - 2aik_\xi}}, \tag{27}$$

wherein $K = \sqrt{k_y^2 + k_\xi^2}$, $a = v/2\alpha$. Now, substituting (23) and (28) into (17), we find the Fourier coefficients for the homogeneous solution, as follows:

$$C_k = \frac{F(k_y, k_\xi)}{\beta + \sqrt{K^2 - 2iak_\xi}}. \tag{28}$$

A homogeneous solution with correct boundary conditions can be written as the following integral (δ-functions in F are explicitly integrated):

$$T_h(\xi, y, z) = T_0 - \frac{\beta p}{8\pi^2\alpha}\int_{-\infty}^{+\infty}\int_{-\infty}^{+\infty} dk_y dk_\xi \frac{e^{i(k_\xi\xi + k_y y) + \sqrt{K^2 - 2iak_\xi}\, z}}{\sqrt{K^2 - 2iak_\xi}\left(\beta + \sqrt{K^2 - 2iak_\xi}\right)}. \tag{29}$$

As further analysis shows, formula (29) does not enable any transformation that would enable the result to be presented in an analytical form, either partially or completely free of quadratures. Therefore, all further illustrations will be obtained using numerical Fourier transformation for specific values of the model parameters.

First, let us write down the complete solution with the correct boundary conditions using formula (16):

$$\begin{aligned} T(\xi, y, z) = T_0 - \frac{\beta p}{8\pi^2\alpha}\int_{-\infty}^{+\infty}\int_{-\infty}^{+\infty} dk_y dk_\xi \frac{e^{i(k_\xi\xi + k_y y) + \sqrt{K^2 - 2iak_\xi}\, z}}{\sqrt{K^2 - 2iak_\xi}\left(\beta + \sqrt{K^2 - 2iak_\xi}\right)} + \\ + \frac{p}{4\pi\alpha} \cdot \frac{e^{-\left(\sqrt{\xi^2 + y^2 + z^2} + \xi\right)v/2\alpha}}{\sqrt{\xi^2 + y^2 + z^2}}, \end{aligned} \tag{30}$$

wherein $\xi = x - vt$.

Let us assume the following average values for the model parameters (in the SI system):

$$T_0 = 300,\ a = 40,\ \frac{p}{4\pi a} = 10^3,\ \beta = 2\pi \cdot 10^{-2},\ v = 10^{-3}.$$

Next, we note that the parameter β (which has the dimension of a wave number, i.e., the reciprocal of the wavelength) in formula (30) can be considered small. In this case, the solution will differ significantly for the region $k \to 0$, which corresponds to the long-wave modes of the solution describing regions of medium distance from the source. Thus, a simplified form of formula (30) is obtained by neglecting β in the denominator under the integral—this corresponds to the preservation of first-order terms in the expansion of the solution with respect to

parameter β (even in this case, the integrals are not calculated analytically). As a result, switching to the real form of the Fourier transform for convenience of calculation, we find

$$T(\xi,y,z)=300-100\int\limits_{-\infty}^{+\infty}\int\limits_{-\infty}^{+\infty}dk_y dk_\xi\frac{2e^{Q_+ z/\sqrt{2}}}{K^4+6400k_\xi^2}\times$$
$$\times\left(K^2\cos(k_\xi\xi+k_y y-c\,\mathrm{sgn}(k_\xi)Q_- z)-80k_\xi\sin(k_\xi\xi+k_y y-c\,\mathrm{sgn}(k_\xi)Q_- z)\right)+10000\frac{e^{-40\left(\sqrt{\xi^2+y^2+z^2}+\xi\right)}}{\sqrt{\xi^2+y^2+z^2}}, \quad (31)$$

wherein

$$Q_\pm=\sqrt{\sqrt{K^4+6400k_\xi^2}\pm K^2},\ \xi=x-10^{-3}t.$$

Let us move on to illustrations of dependence (31). Figures 3 and 4 show families of one-dimensional graphs obtained from the complete dependence (31). The family of curves in Fig. 3 represents the evolution of temperature over time at points in the medium located at different depths in the thickness of the medium below the origin of the coordinate system. The graphs show that sometime after passing the heating pulse, the temperature inside the medium reaches its maximum value rapidly, and then it slowly relaxes to the ambient temperature. At the same time, along with its penetration deeper into the medium, the thermal pulse is spreading out. As a result, its amplitude decreases and its width increases, and the time it takes to reach its maximum value increases monotonically. Overall, this picture corresponds to all physically reasonable expectations of the model under consideration.

Figure 4 shows the spatial distribution of temperature at time $t = 0$ in the bulk of the substance under the heat line—the straight trajectory of the candle flame—depending on the longitudinal coordinate x at the same depths z, similar to that in Fig. 3. At the moment in question, the candle passes over the point $x = 0$. It can be seen that the thermal impulse (which is more pronounced the closer the point in question is to the surface) has accumulated in the previous section $x < 0$ and will continue to move to the right in accordance with the dependencies in Fig. 3.

The transverse temperature distribution relative to the thermal line is represented by a family of graphs in Fig. 5. It has the expected appearance of symmetrical peaks, which become less sharp the deeper the observation point is located.

The obtained solution (16) can be used when describing the temperature field some distance away from the action area of the candle, where specific heating details (e.g., temperature distribution at the initial spray spot) are not apparent. In particular, the graphs in Fig. 4 show that significant temperature gradients arise in the vicinity of the action area of the candle, which will cause noticeable nonstationary temperature stresses. Their relaxation in the vicinity of the passed sections of the thermal line will, in one way or another, affect the quality of the coating, which can probably be controlled technologically by means of special spraying timing, coordinated with the dynamics of the temperature wave in the layer.

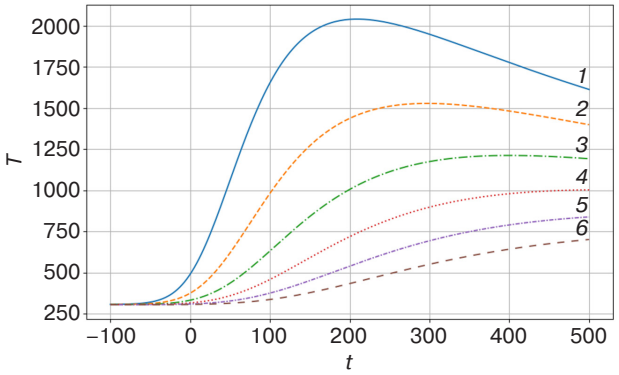

Fig. 3. Temporal evolution of temperature at points with the coordinates $x = y = 0$: (*1*) $z = -0.1$ mm, (*2*) $z = -0.2$ mm, (*3*) $z = -0.3$ mm, (*4*) $z = -0.4$ mm, (*5*) $z = -0.5$ mm, (*6*) $z = -0.6$ mm. The negative time corresponds to the accepted asymptotic initial condition (5); in a moving coordinate system, the moment $t = 0$ is conditional

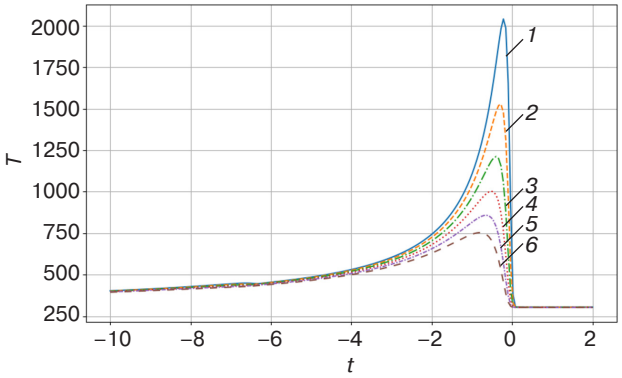

Fig. 4. Spatial profile of the temperature wave at $y = 0$, $t = 0$ as a function of coordinate x at the same depths in the layer as in Fig. 3: (*1*) $z = -0.1$ mm, (*2*) $z = -0.2$ mm, (*3*) $z = -0.3$ mm, (*4*) $z = -0.4$ mm, (*5*) $z = -0.5$ mm, (*6*) $z = -0.6$ mm

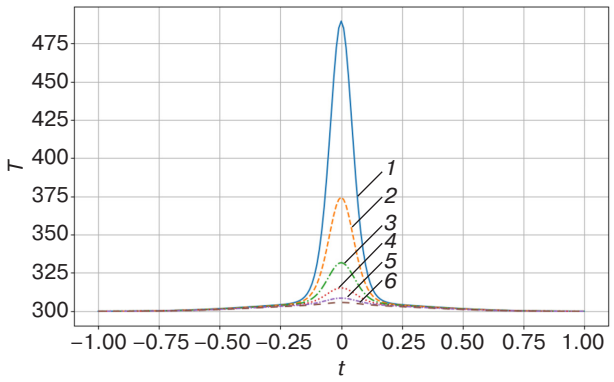

Fig. 5. Transverse spatial profile of the temperature wave at $x = 0$, $t = 0$ as a function of the y coordinate at the same depths in the layer as in Fig. 3:
(*1*) $z = -0.1$ mm, (*2*) $z = -0.2$ mm,
(*3*) $z = -0.3$ mm, (*4*) $z = -0.4$ mm,
(*5*) $z = -0.5$ mm, (*6*) $z = -0.6$ mm

CONCLUSIONS

This article addresses a nonstationary heat conduction problem simulating the technology of gas-thermal spraying of a thin strip forming part of a protective coating. An exact analytical solution describing the temperature field in the substrate material during the movement of a plasma torch creating a heat strip is obtained.

Our calculations showed that:

- after passing the heating pulse, the temperature inside the medium reaches rapidly its maximum value and then relaxes slowly to the ambient temperature;
- when penetrating deeper into the material, the thermal pulse spreads out, reducing its amplitude and increasing its width, while the time it takes to reach the maximum temperature increases;
- significant temperature gradients occur in the vicinity of the heat source, which can lead to nonstationary thermal stresses.

These facts are fully consistent with the general laws of thermophysical processes and, taken together, demonstrate the correctness of the selected physical model and the validity of the approximations made.

An accurate formula for the temperature field of a nonstationary heat strip was derived, enabling a detailed theoretical investigation of all essential characteristics of the heat pulse and their use in calculating experimentally and practically significant parameters of the spraying technology. It should be noted that the experimental possibilities for investigating the characteristics of the heat pulse under the conditions considered are rather limited and resource-intensive.

The resulting solution can be useful for describing the general temperature field at a certain distance from the spray head, where the details of the thermal band structure are not apparent. The results can be used to optimize the technological parameters of spraying, such as spraying timing, in order to control the quality of the coating obtained.

Authors' contribution
All authors contributed equally to the research work.

REFERENCES

1. Davis J.R. *Handbook of Thermal Spray Technology*. ASM International; 2004. 338 p.
2. *Gazotermicheskoe napylenie* (*Gas Thermal Spraying*). Baldaev L.H. (Ed.). Moscow: Market DS; 2007. 344 p. (in Russ.).
3. Ghasempour-Mouziraji M., Lagarinhos J., Afonso D., de Sousa R.A. A review study on metal powder materials and processing parameters in Laser Metal Deposition. *Opt. Laser Technol*. 2024;170:110226. https://doi.org/10.1016/j.optlastec.2023.110226
4. Cheng J., Xing Y., Dong E., Zhao L., Liu H., Chang T., Chen M., Wang J., Lu J., Wan J. An Overview of Laser Metal Deposition for Cladding: Defect Formation Mechanisms, Defect Suppression Methods and Performance Improvements of Laser-Cladded Layers. *Materials*. 2022;15(16):5522. https://doi.org/10.3390/ma15165522
5. Chen H.F., Zhang C., Liu Y.C., Song P., Li W.-X., Yang G., Liu B. Recent progress in thermal/environmental barrier coatings and their corrosion resistance. *Rare Met*. 2020;39(5):498–512. https://doi.org/10.1007/s12598-019-01307-1
6. Hardwicke C.U., Lau Y.C. Advances in Thermal Spray Coatings for Gas Turbines and Energy Generation: A Review. *J. Therm. Spray Technol*. 2013;22(5):564–576. https://doi.org/10.1007/s11666-013-9904-0
7. Bernhard R., Neef P., Wiche H., Wesling V., Hoff C., Hermsdorf J., Kaierle S. Laser Cladding – Additive Manufacturing. In: Cavaliere P. (Ed.) *Laser Cladding of Metals*. Springer, Cham; 2021. P. 1–8. https://doi.org/10.1007/978-3-030-53195-9_1
8. Lim W.Y.S., Cao J., Suwardi A., Meng T.L., Tan C.K.I., Liu H. Recent advances in laser-cladding of metal alloys for protective coating and additive manufacturing. *J. Adhes. Sci. Technol*. 2022;36(23–24):2482–2504. https://doi.org/10.1080/01694243.2022.2085499
9. Zhuravskiy A.V. Mathematical Modeling of Heat Transfer During Chemical Vapor Deposition. *Izvestiya vysshikh uchebnykh zavedenii. Mashinostroenie = BMSTU Journal of Mechanical Engineering*. 2017;11(692):10–17 (in Russ.). https://doi.org/10.18698/0536-1044-2017-11-10-17

10. Ravichandran K.S., An K., Dutton R.E., Semiatin S.L. Thermal conductivity of plasma-sprayed monolithic and multilayer coatings of alumina and yttria-stabilized zirconia. *J. Am. Ceram. Soc*. 2004;82(3):673–682. https://doi.org/10.1111/j.1151-2916.1999.tb01816.x
11. Ma K., Cheng Y., Jeyaprakash N., Zhou J., Wan Y., Yang W. Temperature gradient and solidification rate simulation model of the microstructure of laser-cladded 27SiMn. *Metals*. 2023;13(10):1682. https://doi.org/10.3390/met13101682
12. Moritz S., Schwanekamp T., Reuber M., Lentz J., Boes J., Weber S. Impact of *in situ* heat treatment effects during laser-based powder bed fusion of 1.3343 high-speed steel with preheating temperatures up to 700 °C. *Steel Research Int*. 2023;94(6):2200775. https://doi.org/10.1002/srin.202200775
13. Yamashita Y., Ilman K.A., Kunimine T., Sato Y. Temperature evaluation of cladding beads and the surrounding area during the laser metal deposition process. *J. Manuf. Mater. Process*. 2023;7(6):192. https://doi.org/10.3390/jmmp7060192
14. Chen C., Sun G., Ren B., Wang H., Zhang Y., Zhao X. A novel heterogeneous particle addition method based on laser cladding hybrid wire arc additive manufacturing: improvement performance of stainless steel components. *Virtual Phys. Prototyp*. 2024;19(1):e2397815 https://doi.org/10.1080/17452759.2024.2397815
15. Li C., Han X., Zhang D., Gao X., Jia T. Quantitative analysis and experimental study of the influence of process parameters on the evolution of laser cladding. *J. Adhes. Sci. Technol*. 2021;36(17):1894–1920. https://doi.org/10.1080/01694243.2021.1991142
16. Li C., Jia T., Han X., Jiang X. Study on parameter optimization of laser cladding Fe60 based on GA-BP neural network. *J. Adhes. Sci. Technol*. 2022;37(18):2556–2586. https://doi.org/10.1080/01694243.2022.2159298
17. Huang H., Wu M., Luo S., Chen Z. Optimization of process parameters in laser cladding multi channel forming using MVBM-NSGA-II method. *Mater. Manuf. Processes*. 2024;39(15):2226–2235. https://doi.org/10.1080/10426914.2024.2395002
18. Hu Z., Li C., Tian D., Li X., Wang J., Xu Z., Sun X. Numerical simulation analysis of temperature distribution of NbC-reinforced Ti-based composite coating by laser cladding. *Metals*. 2023;13(8):1348. https://doi.org/10.3390/met13081348
19. Deng C., Zhu Y., Chen W. Numerical Investigation of the Effects of Process Parameters on Temperature Distribution and Cladding-Layer Height in Laser Cladding. *Coatings*. 2024;14(8):1020. https://doi.org/10.3390/coatings14081020
20. Jiang Y., Cheng Y., Zhang X., Yang J., Yang X., Cheng Z. Simulation and experimental investigations on the effect of Marangoni convection on thermal field during laser cladding process. *Optik.* 2020;203:164044. https://doi.org/10.1016/j.ijleo.2019.164044
21. Sun Z., Guo W., Li L. Numerical modelling of heat transfer, mass transport and microstructure formation in a high deposition rate laser directed energy deposition process. *Addit. Manuf.* 2020;33:101175. https://doi.org/10.1016/j.addma.2020.101175
22. Wang C., Zhou J., Zhang T., Meng X., Li P., Huang S. Numerical simulation and solidification characteristics for laser cladding of Inconel 718. *Opt. Laser Technol*. 2022;149:107843. https://doi.org/10.1016/j.optlastec.2021.107843
23. Chai Q., Zhang H., Fang C., Qiu X., Xing Y. Numerical and experimental investigation into temperature field and profile of Stellite6 formed by ultrasonic vibration-assisted laser cladding. *J. Manuf. Process.* 2023;85:80–89. https://doi.org/10.1016/j.jmapro.2022.11.035
24. de La Batut B., Fergani O., Brotan V., Bambach M., Mansouri M.E. Analytical and numerical temperature prediction in direct metal deposition of Ti6Al4V. *J. Manuf. Mater. Process*. 2017;1(1):3. https://doi.org/10.3390/jmmp1010003
25. Gao Y., Jiang S., Tong Y., Bai S., Lu P. Temperature field simulation and experimental confirmation of laser cladding high-entropy alloy coating on Cr12MoV. *Processes*. 2024;12(2):257. https://doi.org/10.3390/pr12020257

About the Authors

Mikhail E. Soloviev, Dr. Sci. (Phys.-Math.), Professor, Department of Information Systems and Technologies, Institute of Digital Systems, Yaroslavl State Technical University (88, Moskovskii pr., Yaroslavl, 150023 Russia). E-mail: me_s@mail.ru. Scopus Author ID 57190224257, ResearcherID A-4328-2014, RSCI SPIN-code 7444-3564, https://orcid.org/0000-0002-8840-248X

Sergey S. Kokarev, Cand. Sci. (Phys.-Math.), Director of the Regional Scientific and Educational Center "Logos" (80, Respublikanskaya ul., Yaroslavl, 150000 Russia). E-mail: logos-center@mail.ru. https://orcid.org/0000-0001-6944-1400

Sergey L. Baldaev, Cand. Sci. (Eng.), Deputy General Director, Technological Systems for Protective Coatings (9A, Yuzhnaya ul., Shcherbinka, Moscow, 108851 Russia). E-mail: s.baldaev@tspc.ru. ResearcherID B-8056-2018, RSCI SPIN-code 6954-6407, https://orcid.org/0000-0002-1917-7979

Lev Kh. Baldaev, Dr. Sci. (Eng.), General Director, Technological Systems for Protective Coatings (9A, Yuzhnaya ul., Shcherbinka, Moscow, 108851 Russia). E-mail: l.baldaev@tspc.ru. RSCI SPIN-code 8991-5015, https://orcid.org/0000-0002-9084-8771

Denis V. Malyshev, Assistant, Department of Information Systems and Technologies, Institute of Digital Systems, Yaroslavl State Technical University (88, Moskovskii pr., Yaroslavl, 150023 Russia). E-mail: deniscs49@gmail.com. https://orcid.org/0009-0009-9861-1531

Об авторах

Соловьев Михаил Евгеньевич, д.ф.-м.н., профессор, кафедра информационных систем и технологий, Институт цифровых систем, ФГБОУ «Ярославский государственный технический университет» (150023, Россия, Ярославль, Московский пр-т, д. 88). E-mail: me_s@mail.ru. Scopus Author ID 57190224257, ResearcherID A-4328-2014, SPIN-код РИНЦ 7444-3564, https://orcid.org/0000-0002-8840-248X

Кокарев Сергей Сергеевич, к.ф.-м.н., директор регионального научно-образовательного центра «Логос» (150000, Россия, Ярославль, ул. Республиканская, д. 80). E-mail: logos-center@mail.ru. https://orcid.org/0000-0001-6944-1400

Балдаев Сергей Львович, к.т.н., заместитель генерального директора по технологиям, ООО «Технологические системы защитных покрытий» (108851, Россия, Москва, г. Щербинка, ул. Южная, д. 9А). E-mail: s.baldaev@tspc.ru. ResearcherID B-8056-2018, SPIN-код РИНЦ 6954-6407, https://orcid.org/0000-0002-1917-7979

Балдаев Лев Христофорович, д.т.н., генеральный директор ООО «Технологические системы защитных покрытий» (108851, Россия, Москва, г. Щербинка, ул. Южная, д. 9А). E-mail: l.baldaev@tspc.ru. SPIN-код РИНЦ 8991-5015, https://orcid.org/0000-0002-9084-8771

Малышев Денис Владимирович, ассистент, кафедра информационных систем и технологий, Институт цифровых систем, ФГБОУ «Ярославский государственный технический университет» (150023, Россия, Ярославль, Московский пр-т, д. 88). E-mail: deniscs49@gmail.com. https://orcid.org/0009-0009-9861-1531

Translated from Russian into English by Lyudmila O. Bychkova
Edited for English language and spelling by Dr. David Mossop